Analysis and Modeling of Sintering of Sr-hexaferrite Produced by PIM Technology

B. S. Zlatkov[1], M.V. Nikolic[2*], V. Zeljkovic[3], N. Obradovic[3], V. B. Pavlovic[3], O. Aleksic[2]

[1]Volkswagen Aktiengesellschaft, D-38436 Wolfsburg, Germany
[2]Institute for Multidicsciplinary Research, Kneza Viseslava 1, 11000 Beograd, Serbia
[3]Institute of Technical Sciences of SASA, Knez Mihailova 35, 11000 Beograd, Serbia

_____

Abstract:
     The powder injection moulding (PIM) technology is lately becoming more and more significant due to complex design possibilities and good repeatability. This technology requires optimization of all steps starting with material and binder, injection, debinding and sintering parameters. Sintering is one of the key links in this technology. The powder injection moulding process is specific as during feedstock injection powder particles mixed into the binder do not come into mechanical contact. Shrinkage during sintering of PIM samples is high. In this work we have analyzed and modeled the sintering process of isotropic PIM samples of Sr-hexaferrite. The Master Sintering Curve (MSC) principle has been applied to analyze sintering of two types of PIM Sr-hexaferrite samples with completely removed binder and only the extraction step of the debinding procedure (thermal debinding proceeding simultaneously with sintering). Influence of the heating rate on resulting sample microstructures has also been analyzed. Influence of the sintering time and temperature was analyzed using three different phenomenological equations.
Keywords: Sintering, Modeling, Sr-hexaferrite, PIM technology.
_____

1. Introduction

     Hard ferrites are used today mainly for the production of different permanent magnetic cores. Sintered ferrite cores are not well suited for additional mechanical treatment such as cutting and grinding to fit the tolerances, and because of that a "near net shape" technology such as PIM (powder injection molding) is an attractive alternative [1, 2]. Hard ferrites - "hexaferrites" are based on Fe_2O_3 and metal oxides - MO (M = Pb, Ba, Sr) and have a hexagonal structure (M-type magnetoplumbite, space group $P6_3/mmc$). $BaFe_{12}O_{19}$ and $SrFe_{12}O_{19}$ are used most often [3-6]. These ferromagnetic materials can be easily magnetized along the *c*-axis. Application of a high intensity magnetic field in the injection phase during powder injection moulding results in magnetic alignment and a saturated orientation of single domain hexaferrite particles in parallel to the c-axis. Once oriented during injection, the particles remain oriented during debinding and sintering. [7-10]. Optimization of all steps of the PIM process is very significant. This includes selection of a suitable feedstock followed by optimization of debinding and sintering processes.
     Sintering is a complex process involving several diffusion mass transport mechanisms

_____
*) Corresponding author: mariav@rcub.bg.ac.rs

[11]. Many different models and approaches have been developed to describe the sintering process [12-14]. The aim of these models is to enable prediction of the properties of sintered samples. Modeling of densification during sintering of PIM samples will enable selection of a suitable sintering window, i.e. optimal sintering temperature – hold time regime in order to achieve optimal properties. Modeling of the sintering process of PIM magnetic materials needs to include optimization of sintering parameters in order to obtain maximal sample density. It must take into account the presence of a residual binder and its influence on the sintering process. Another problem, due to different complex shapes of PIM samples, is that shrinkage during sintering is not necessarily the same along all sample dimensions especially in the case of magnetically aligned PIM samples.

For most materials either grain boundary or volume diffusion are the dominant densification mechanism during sintering. According to Su and Johnson [12] if one diffusion mechanism is dominant, the densification rate can be defined as:

$$\frac{1}{\rho}\frac{d\rho}{dt} = 3\frac{\Omega\gamma D_0}{k_B}\frac{\Gamma(\rho)}{G^n}\frac{e^{-Q/RT}}{T} = A^* F(\rho)^* \theta(T) \qquad (1)$$

where ρ is the relative density, t is time, Ω is the atomic volume, γ is the surface energy, D_0 is the diffusion coefficient, G is the mean grain size, Q is the apparent activation energy, R is the gas constant, T is the absolute temperature and $\Gamma(\rho)$ is a scaling factor describing features in the microstructure characterizing the microstructural geometry. The terms relating to microstructural and materials properties and terms related to the heating schedule are separated and then A includes all constants, $F(\rho) = \Gamma(\rho)/G^n$ and is a function only of density and $\theta(T)$ – the work of sintering, is a function only of temperature, depending on the time-temperature path. The generated master sintering curve (MSC) is unique for a given powder and green body process and is independent of the sintering path and it has been redefined to be a sigmoidal (S-shape) curve [15, 16]:

$$\rho = \rho_0 + \frac{1-\rho_0}{1+\exp\left(-\dfrac{\ln\theta + a}{b}\right)} \qquad (2)$$

where ρ_0 is the relative density at the start of sintering, a and b are constants defining the curve enabling a better fit between the relative sintering density and $\ln\theta$. The master sintering curve (MSC) concept has been applied to analyzing sintering of a wide range of materials: ceramic systems such as alumina [12], nanoscale yttria stabilized zirconia [17], zinc-titanate [18], metal powders such as molybdenum, stainless steel [16,19] and PIM niobium [20].

A phenomenological approach to analysis of the sintering process enables establishment of a functional connection between characteristics of the material and the sintering time and temperature. Phenomenological models are used to most often analyze and model changes of the relative sample density during isothermal sintering in different temperature-time regimes [13, 14]. They have been applied to a wide range of materials. Physical interpretation of the determined parameters has been attempted in terms of defining the dominant diffusion mechanism [13]. Some of the phenomenological models used to analyze the experimentally determined change of the relative sample density as a function of the sintering time (t) at a set sintering temperature are the following [14]:

a) Two-parameter model

$$\frac{\Delta\rho}{\rho} = K_T\left[1 - \exp(-kD \cdot t)\right] \qquad (3)$$

where: K_T, kD are the parameters that need to be determined .

b) Three-parameter model

$$\frac{\Delta\rho}{\rho} = k_e\left[1 - (1+kt)^a\right] \qquad (4)$$

where: $k_e = \left(\dfrac{\Delta\rho}{\rho}\right) = \dfrac{\rho_T - \rho_0}{\rho_T}$, and k, k_e , a are parameters that need to be determined.

c) General process equation (Ristic-Jovanovic [21])

$$\frac{\Delta\rho}{\rho} = k_0 \cdot \left(1 - B \cdot e^{-s \cdot t}\right) \cdot (s \cdot t)^{\exp\left[-\frac{1}{2}\left(p^2 \cdot t^2 - 1\right)\right]} \tag{5}$$

where: k_0 , B , S and p are parameters that need to be determined.

Parameters K_T, k_e , k_0 refer to the total change in relative density (for longer sintering times) on a certain sintering temperature. Other parameters given in these three equations influence the process rate, i.e. gradient changes of relative density as a function of the sintering time. The number of parameters used in the model is very significant. Increase of the number of parameters gives the model greater flexibility and better adjustment to experimental data. On the other hand, more parameters require a more complex mathematical program and parameter determination process. It is significant that the applied model and determined parameters describe well the process in the field significant for practical applications.

The purpose of this work was to analyze the sintering process of PIM strontium hexaferrite using different models and starting samples. Optimization of the sintering time-temperature regime was viewed using phenomenological models analyzing the relative change in sample density during isothermal sintering of samples that had previously underwent the complete debinding procedure. The influence of binder presence in the PIM strontium hexaferrite samples and the sample heating rate were analyzed using the master sintering curve approach.

2. Experimental procedure

Powder and feedstock preparation

Starting Sr-hexaferrite powder (Tridelta, Germany) was produced by dry mixing of hematite Fe_2O_3 (99.9%, Aldrich) and strontium carbonate $SrCO_3$ (99%, Sigma-Aldrich) followed by calcinations at 1000°C for 2 h in air and then milling for 24 h in slow ball mills. A Fisher Subsieve Sizer was used to measure the resulting particle size that was found to be $d_{50} < 1.25$ μm. A scanning electron microscope (SEM) image of the starting powder (taken on a TESCAN Electron Microscope VEGA TS 5130mm) is given in fig. 1. The main properties of the powder used are given in Tab. I.

Tab. I Specification of $SrFe_{12}O_{19}$ starting powder

Production method		Calcination
Chemical formula		$SrFe_{12}O_{19}$
Mole ratio	$SrO : Fe_2O_3$	1:5.7
Theoretical density	[g/cm^3]	5.10
Apparent density	[g/cm^3]	0.90
Moisture	[%]	0.1
Specific surface area according to Blaine	[cm²/g]	ca. 4600
Crystal structure/Space group		Hexagonal P6$_3$/mmc
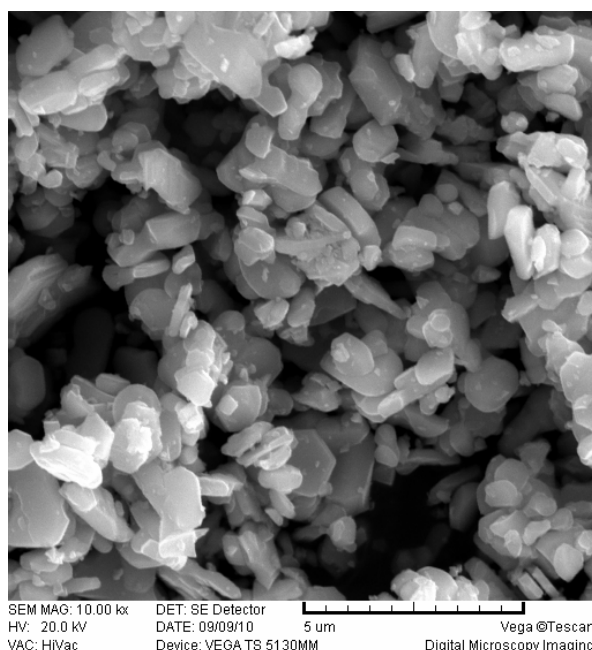
Fig. 1. SEM image of $SrFe_{12}O_{19}$ starting powder

Feedstock was prepared by mixing as-milled Sr-Ferrite powder with a "Solvent System" binder containing mainly wax, thermoplastics and additives

Injection moulding, debinding and sintering

A Battenfeld HM 600/130 hydraulic drive injection moulding machine was used for this investigation. Powder injection moulding parameters used are given in Tab. II. The resulting green cylindrical component with a central hole has the following dimensions: external diameter $d = 18$ mm, internal diameter $D = 10$ mm and height $H = 28$ mm. Two grooves are symmetrically positioned at an angle of 180°.

Tab. II Powder injection moulding (PIM) parameters.

PIM Parameter		
Injection temperature	[°C]	145
Tool temperature	[°C]	35
Back pressure [MPa]		6
Flow rate [cm³/s]		10
Injection pressure [MPa]		105
Holding pressure [MPa]		70
Holding time	[s]	3
Filling time	[s]	2.27
Cooling time	[s]	25

After shaping of green parts by injection moulding, debinding was performed in two steps. The first step of debinding was done by extraction with acetone in a MDU-60 furnace produced by DesbaTec Anlagentechnik GmbH, Sulzbach, Germany. The optimal time of extraction was about 16 h at 45°C. The resulting parts were then dried in air at 35°C. Thermal debinding was performed together with sintering in air in a Linn High Therm VMK 1800, Eschenfelden, Germany furnace. Isothermal sintering was performed at three different sintering temperatures: 1200, 1220 and 1240°C for five different sintering hold times 15, 30, 60, 120, 180 and 240min. Sample densities were measured using the Archimedes method with water as a medium. Prior to measurements the samples were impregnated by Erdal AQUA STOPP, Hallein Austria agent. The average green density was determined as 3.23 g/cm^3.

In order to analyze in more detail the shrinkage response, i.e. thermal debinding and sintering of Sr-hexaferrite samples we also performed non-isothermal sintering of two groups of Sr-hexaferrite samples in a Bähr Gerätebau Type 802s dilatometer in a tube furnace. In the first case we sintered green samples of Sr-hexaferrite that had undergone two steps of the debinding procedure: solvent debinding (extraction with acetone) and thermal debinding till 800°C with two isothermal hold time at 300 and 620°C with hold times of 1 h. Sintering of the resulting samples was then performed with a heating rate of 5, 10, 12.5 and 15°C/min, to 1400°C and a hold time of 60 min. In the second case we sintered samples that had only undergone the first debinding step (extraction with acetone) so thermal debinding occurred during sintering. Samples were also sintered to 1400°C with a hold time of 60 min and a heating rate of 3, 7.5 and 10°C/min. Green and sintered sample densities were also measured.

Microstructures of sintered samples were observed on a JEOL JSM 6390LV scanning electron microscope.

3. Results and discussion

The measured dilatometric data for both groups of Sr-hexaferrite samples sintered in a dilatometer are shown in fig. 2. Sample shrinkage is similar for both groups of samples (without and with binder), but the resulting sample density differs significantly. The samples without a binder (group I) had a higher starting density (on average 3.9 g/cm^3 that is 74.5% of the theoretical sample density of Sr-hexaferrite - ρ_T) and the obtained final density was also higher (on average 4.6 g/cm^3 making it 90.2% of ρ_T), compared to group II samples (with binder) where the starting green sample density was 2.8 g/cm^3 (55.1% ρ_T) and the obtained final density was 4.4 g/cm^3 (86.7% ρ_T). These differences are reflected in microstructures of these two groups of samples.

If we analyze the microstructures of Sr-hexaferrite samples (group I) sintered in a dilatometer after thermal debinding, one can note that the microstructures differ in relation to the applied heating rate. If the heating rate is high (15°C/min) the microstrain is high, open and closed porosity is present in the sample, pores have a polygonal shape with an average size 1.5-1.6 μm (fig. 3a). Cracks are also noted, regardless of the relatively high sample density. The pore size distribution is slightly more uniform for the heating rate of 12.5°C/min (fig. 3b) and the average pore size is slightly lower (1-1.2 μm). Breakage through grains, i.e. through splitting planes can also be noted. Pore spheroidization is present in samples sintered with a heating rate of 10°C/min (fig. 3c). Reduction of characteristic growth lines can also be noted and what is most characteristic is spiral concentric grain growth around pores as microstrain is different around them. These characteristic growth lines are also present but less expressed in samples sintered with a heating rate of 5°C/min (fig. 5d). In this case the pores are almost spherical in shape, though slightly hexagonal due to the surrounding hexagonal grains of Sr-ferrite. The average pore size is also lower and on average 500-600 nm. Splitting planes can also be noted.
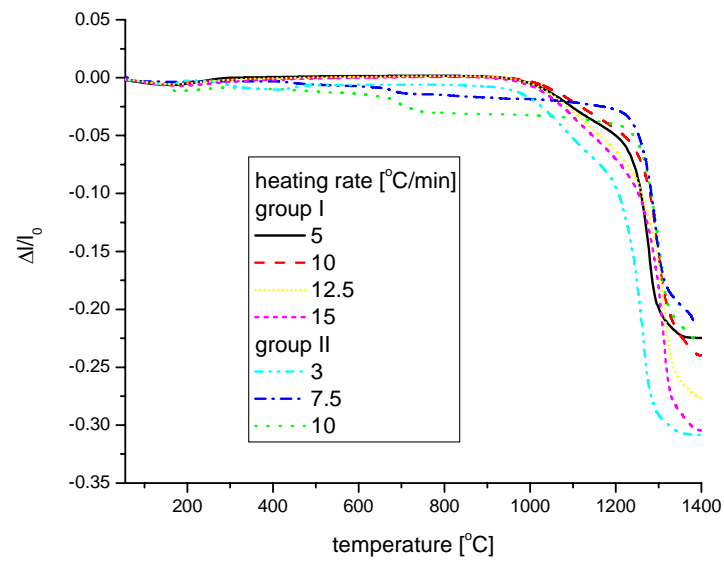
Fig. 2. Linear sample shrinkage as a function of temperature for Sr-hexaferrite samples
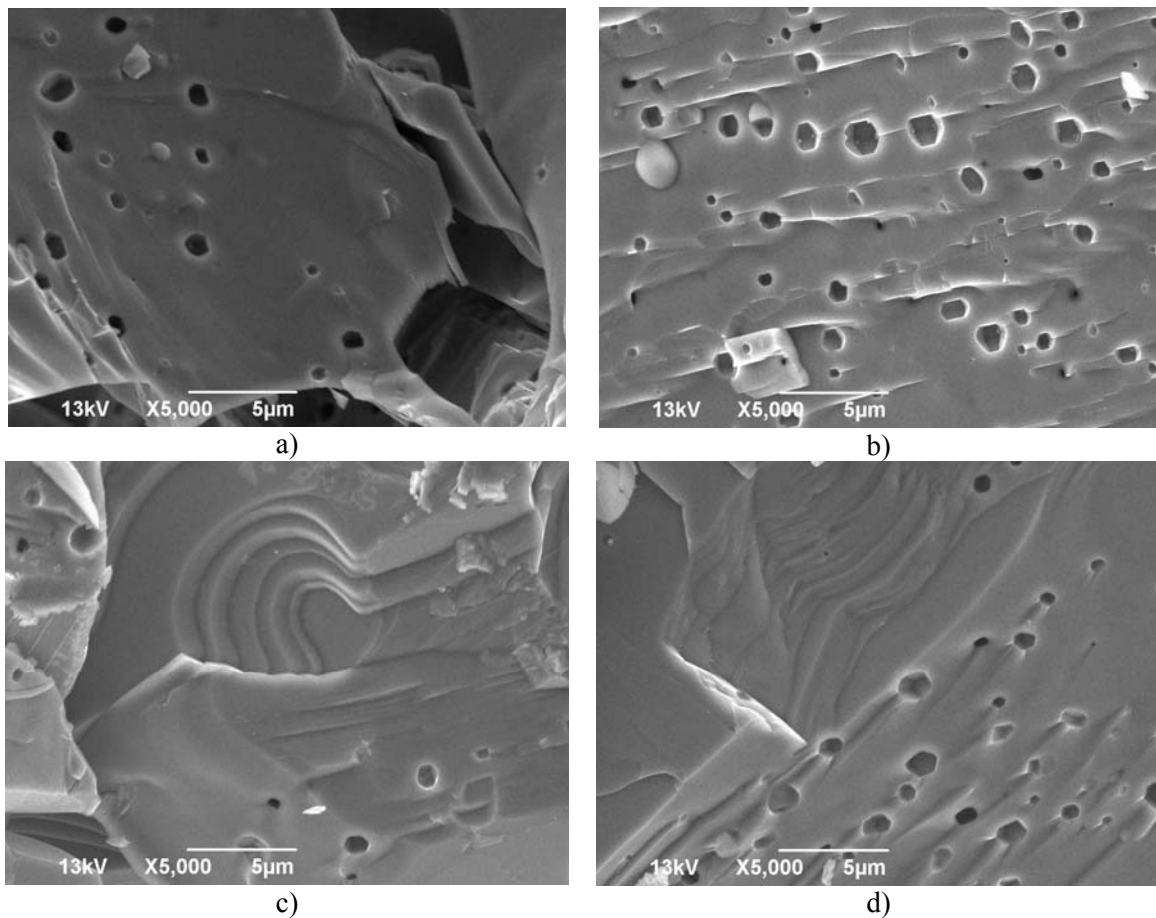
Fig. 3. SEM micrographs of Sr-hexaferrite sintered with heating rates of 15 (a), 12.5 (b), 10 (c) and 5°C/min (d) where debinding was performed on samples prior to sintering

_____

In the case when thermal debinding took place during the initial stages of sintering, for the lowest heating rate of 3°C/min the pore shape and size distribution is varied (fig. 4a). Pore sizes range from 0.5-3 μm. Small cracks can also be noted due to binder evaporation/removal from the sample. When the heating rate is increased to 7.5 μm (fig. 4b) the sample porosity was higher, spiral concentric grain growth is present and the material cracked more noticeably along grain boundaries. Cracks between grains were even more expressed for the heating rate of 10°C/min (fig. 4c). Thus, in order to optimize the debinding/sintering procedure a low heating rate is required, the heating rate of 3°C/min is minimal and lower heating rates than this would probably render even less small cracks.

a)   b)

c)
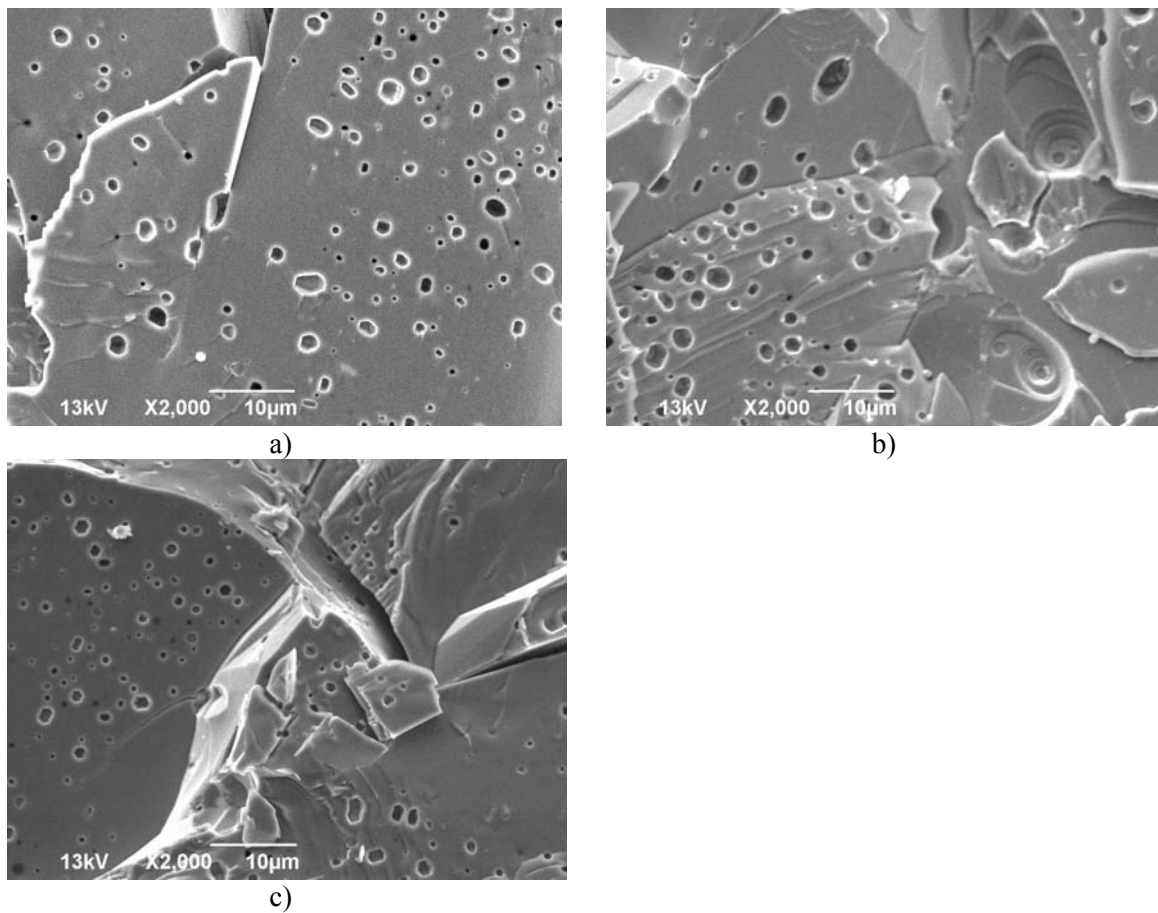
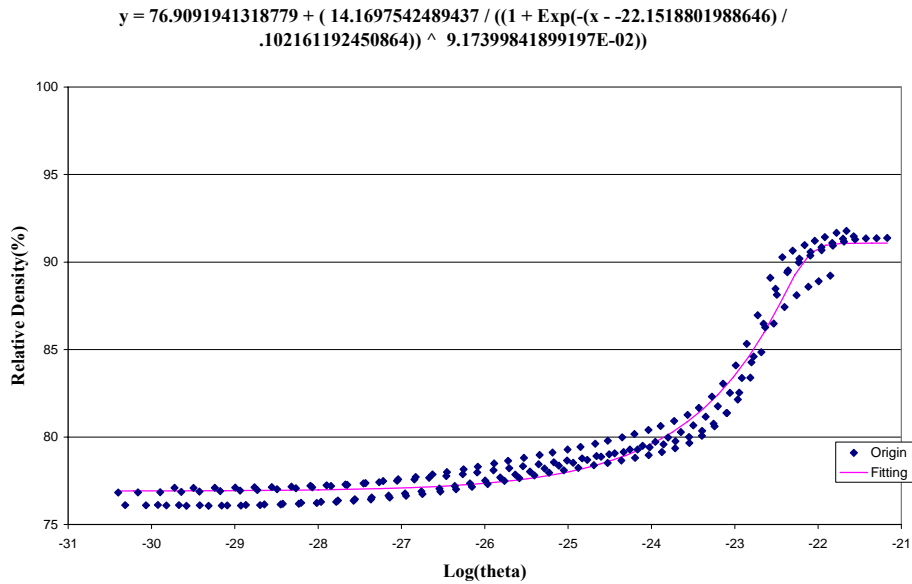**Fig. 4.** SEM micrographs of Sr-hexaferrite sintered with heating rates of 3 (a), 7.5 (b) and 10°C/min

Using shrinkage data obtained from dilatomeric experiments, the sample density was determined as:

$$\rho = \frac{\rho_0}{\left(1 - \alpha \frac{\Delta l}{l_0}\right)^3} \qquad (6)$$
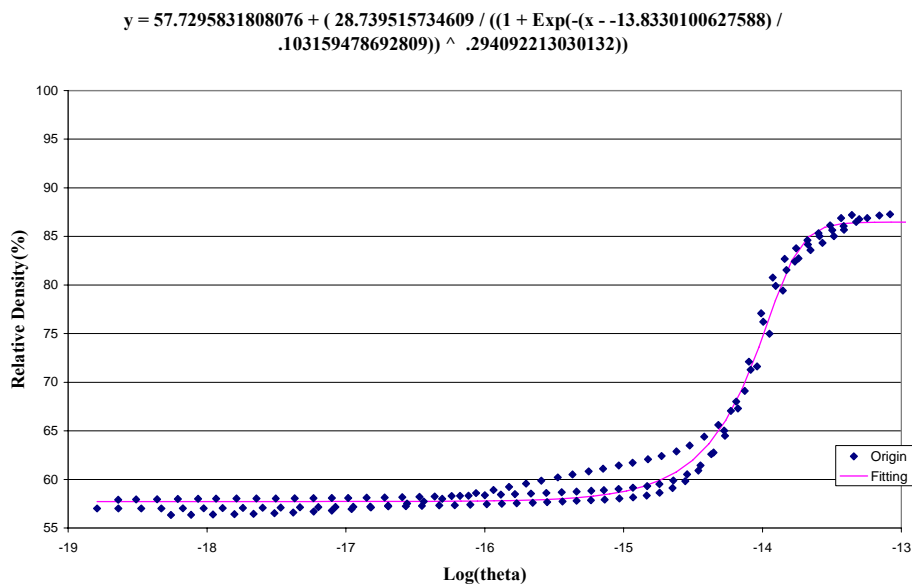
where ρ_0 is the starting green sample density, l_0 is the initial sample length, Δl is the change in sample length, t is the time and, α is the anisotropic shrinkage factor that is calculated for each sample from starting and final sample dimensions.

Two master sintering curves were defined for the analyzed PIM Sr-hexaferrite samples (fig. 5). For the first group of samples where thermal debinding was performed prior

to the sintering experiment the process activation energy was optimized as 655 kJ/mol, while for the second group of samples where thermal debinding occurred during the sintering experiment the process activation energy was determined as 403 kJ/mol. These two curves can be used to predict densification for different sintering temperature – time regimes.

$$y = 76.9091941318779 + (14.1697542489437 / ((1 + Exp(-(x - -22.1518801988646) / .102161192450864)) \wedge 9.17399841899197E-02))$$

Fig. 5a. Master sintering curve for PIM Sr-hexaferrite sintered with heating rates of 15, 12.5, 10 and 5°C/min where debinding was performed on samples prior to sintering

$$y = 57.7295831808076 + (28.739515734609 / ((1 + Exp(-(x - -13.8330100627588) / .103159478692809)) \wedge .294092213030132))$$


Fig. 5b. Master sintering curve for PIM Sr-hexaferrite sintered with heating rates of 10, 7.5 and 3°C/min where debinding was not performed on samples prior to sintering

The measured change of sample density with time and temperature of isothermal sintering is shown in fig 6, where one can see that for all samples the sample density

increased for longer hold times, though after 120 min. this increase was only slight for all applied sintering temperatures. The sample density was the highest for the highest sintering temperature of 1240°C.
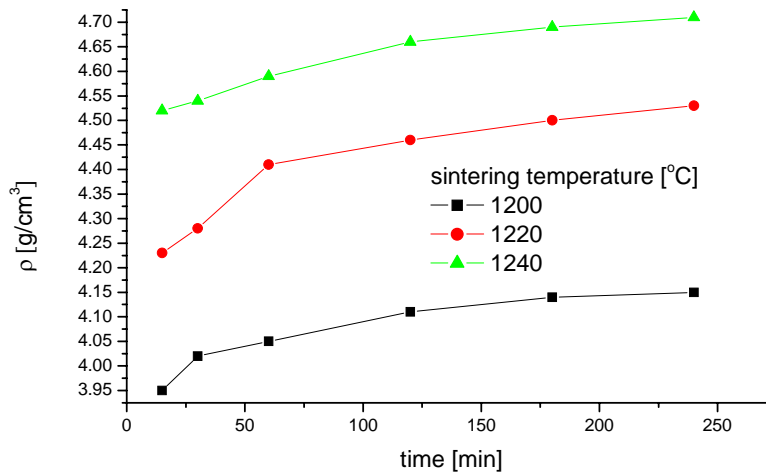

Fig. 6. Change of PIM Sr-hexaferrite sample density with sintering time and temperature

      The experimental data was modeled using the three previously defined phenomenological equations (3-5) as shown in fig. 7 for sintering at 1200°C. One can see that the two-parameter model is not flexible enough and does not follow well enough the experimental data. It is obvious that the general model of Ristic-Jovanovic is the most flexible and follows the experimental data well (fig. 8a). This model has four adjustable parameters. The three parameter model also gives satisfactory results. This can be seen in fig. 8b. The parameters determined using these two models are given in Tab. III.

Tab. III Parameters determined using the three-parameter model
and the Ristic-Jovanovic general equation

Temperature [^{o}C]	1200	1220	1240
Three-parameter model			
Parameters k	-0.6740	-0.7770	-3.260
k_e	0.2280	0.2980	0.3210
a	-0.6500	-0.5900	-0.5300
Ristic-Jovanovic general equation			
Parametri k_0	0.2240	0.2860	0.3180
S	0.0110	0. 0182	0.0098
B	0.1650	0. 2310	0.1210
p	0.1835	1.2215	3.2215

      The total density change at the temperature of T=1240ºC is 31.8%. A rather large density/volume change rate is noted at temperatures around 1200°C. An increase in temperature of 20°C to 1220°C brings about a density change of 6.2%, while a further increase to 1240°C leads to density changes of only 3.2%. This is confirmed by the shrinkage data measured in a dilatometer (fig. 2) where noticeable sample shrinkage starts on average at temperatures between 1100 and 1200°C, regardless of the applied sample heating rate and whether samples have undergone debinding or not.
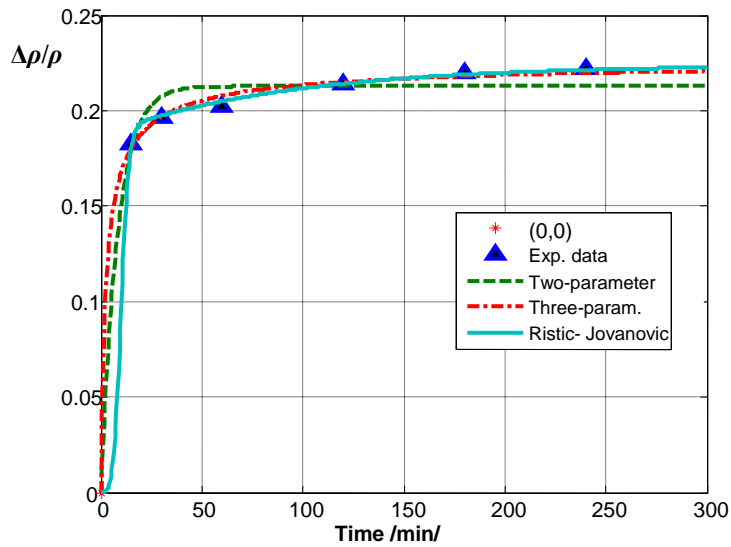
Fig. 7. Comparison of applied phenomenological sintering models: two parameter, three parameter and Ristic Jovanovic on sintering of PIM Sr-hexaferrite at 1200^oC
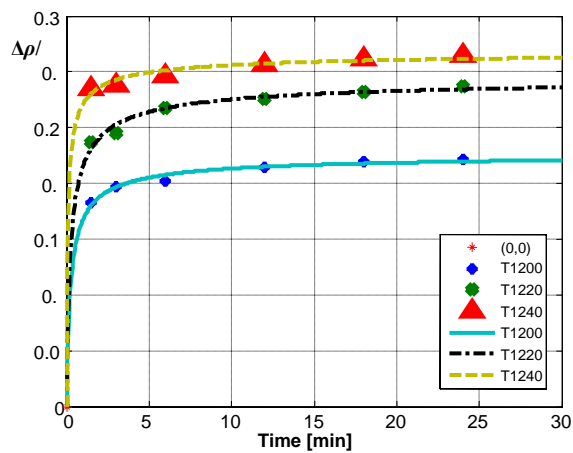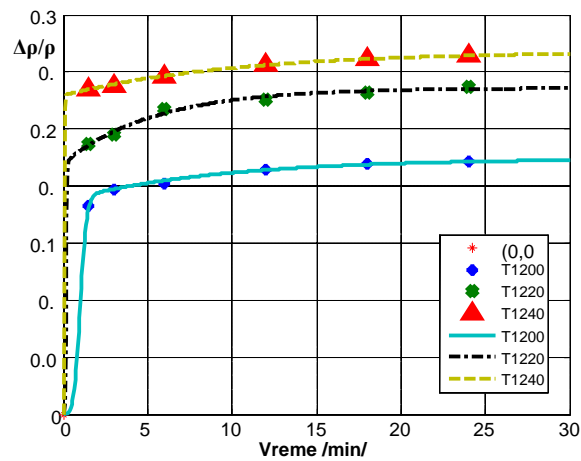
Fig. 8 Ristic-Jovanovic model (a) and three parameter model (b) - change of relative sample density for different sintering temperatures

Determination of the optimal sintering window in the case of PIM magnetic materials, besides resulting sample density, microstructure properties also needs to take into account magnetic properties of the resulting material. Thus, Murillo et al [10] determined the best behaviour with sintering conditions of 1200°C for 2h in air. Introduction of a magnetic field during the feedstock injection process will result in anisotropic samples with improved magnetic properties. Determining the optimal sintering window in view of the applied magnetic field and resulting magnetic properties will be the subject of further work.

4. Conclusion

In this work we analyzed and modeled the sintering process of samples of Sr-ferrite ceramics obtained by PIM technology. Non-isothermal sintering of Sr-hexaferrite samples of two types of samples was analyzed and modeled using the MSC principle. The first group of samples had undergone the complete debinding procedure so only shrinkage during sintering was analyzed and modeled. In the second case the samples had only undergone the first step of the debinding procedure, so the sample shrinkage was higher as it included debinding. Two master sintering curves were obtained and the process activation energies were determined as 655 and 403 kJ/mol for the first and second group of samples, respectively. Sample microstructures also depended on the applied heating rate and sample type. Influence of the isothermal sintering time and temperature were also analyzed and modeled using three different equations. The three parameter model and Ristic-Jovanovic general equation can both be successfully applied. All these analyses of the sintering process of isotropic PIM Sr-hexaferrite samples are the first step in determining optimal sintering windows for different anisotropic magnetically aligned PIM Sr-hexaferrite samples.

5. Acknowledgement

6. References

1. B. S. Zlatkov, E. Griesmayer, H. Loibl, O.S Aleksić, H. Danninger, C. Gierl, L. S. Lukić, Sci. Sintering 40 (2008) 185.
2. M. R. German, A. Bose, Injection molding of metals and ceramics MPIF, Princeton, N.J., 1997.
3. S. Krupicka, Physik der Ferrite und der verwandten magnetischen Oxide, Verlag der tschechoslowakischen Akademie der Wissenschaften, Praha 1973
4. A. Goldman, Modern ferrite technology, Springer, 2006.
5. R.C.O. Handley, Modern magnetic materials, principles and applications, John Wiley&Sons, NY (2000), 485-491
6. G. Heimke, Keramische Magnete, Springer-Verlag 1976.
7. B. S. Zlatkov, Ph.D. Thesis, Technische Universitaet Wien, 2008.
8. B. S. Zlatkov, M. V. Nikolic, O. Aleksic, H. Danninger, E. Halwax, J. Magn. Magn. Mater. 321 (2009) 330.

9. S. H. Lee, W. Y. Jeung, J. Magn. Magn. Mater. 226-230 (2001) 1400.
10. N. Murillo J. González, C. Guraya, M. Gutiérrez F. J. Seco, J Magn. Magn. Mater. 203 (1999) 165.
11. D. Lance, F. Valdivieso, P. Goueriot, J. Eur. Ceram. Soc. 24 (2004) 2749.
12. H. Su, D. L. Johnson, J. Am. Ceram. Soc. 79 (1996) 3211.
13. V. Zeljkovic, Mathematical Analysis of Sintering Laws of Real Materials, Belgrade, Serbian Academy of Sciences and Arts, 2007.
14. M. V. Nikolic, N. Labus, Materials Science Forum, 453-454 (2004) 441.
15. M.-H. Teng, Y.-C. Lai, Y.-T. Chen, Westr. Pac. Earth Sci. 2 (2002) 171.
16. D. C. Blaine, J. R. Gurosik, S. J. Park, D. F. Heaney, R. M. German, Metall. Mater. Trans. A 37A (2006) 715.
17. M. Mazaheri, A. Simchi, M. Dourandish, F. Golestani-Fard, Ceram. Int. 35 (2009) 547.
18. M. V. Nikolic, N. Labus, M. M. Ristic, Ceram. Int. 35 (2009) 3217.
19. D. C. Blaine, S. J. Park, P. Suri, R. M. German, Metall. Mater. Trans. A 37A (2006) 2827.
20. G. Aggarwal, I. Smid, S. J. Park, R. M. German, Int. J. Refract. Met. H. 25 (2007) 226.
21. M. M. Ristic, S. Jovanovic, Poroshkovaya Metallurgiya, 9 (1967) 102.

Садржај: *Технологија обликовања праха бризгањем (ПИМ) постаје све значајнија узимајући у обзир могућности дизајна комплексних облика и добру поновљивост. Ова технологија тражи оптимизацију свих корака од материјала, везива, као и параметера бризгања, уклањања везива и синтеровања. Синтеровање представља један од основних делова ове технологије. ПИМ процес је специфичан јер током бризгања фидстока честице праха које су измешане у везиву не долазе у механички контакт. Скупљање током синтеровања ПИМ узорака је велико. У овом раду смо анализирали и моделовали процес синтеровања изотропских ПИМ узорака стронцијум хексаферита. Принцип мастер криве синтеровања је примењен за анализу две групе ПИМ стронцијум хексаферитних узорака, где је везиво комплетно одстрањено и где је само извршена екстракција везива а процес термичког одстрањивања везива се дешава заједно са синтеровањем. Утицаји времена синтеровања и температуре су анализирани коришћењем три различите феноменолошке једначине.*
Кључне речи: *Синтеровање, моделовање, Sr-хексаферит, ПИМ технологија.*